Dalton Transactions

Accepted Manuscript

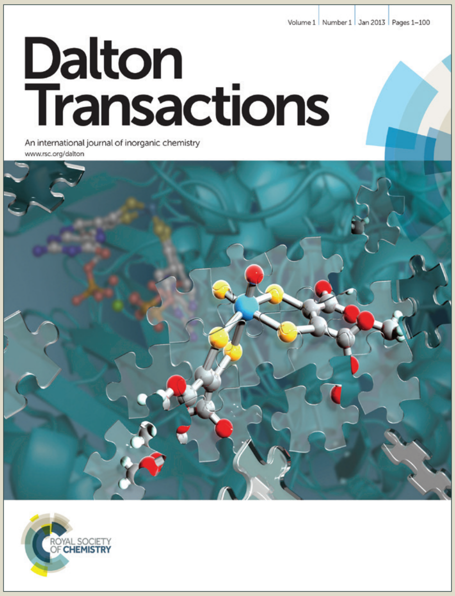

ROYAL SOCIETY OF CHEMISTRY

www.rsc.org/dalton

$[Mn_2Ga_4Sn_4S_{20}]^{8-}$ T3 Supertetrahedral Nanocluster Directed by a Series of Transition Metal Complexes

Cheng-Yang Yue,* Xiao-Wu Lei,* Li-Juan Feng, Chen Wang, Ya-Ping Gong,

Xin-Ying Liu

Key Laboratory of Inorganic Chemistry in Universities of Shandong, Department of Chemistry and Chemical Engineering, Jining University, Qufu, Shandong, 273155, China

*Corresponding author: Cheng-Yang Yue, Xiao-Wu Lei

E-mail address: yuechengyang@126.com

xwlei_jnu@163.com

Abstract: With different transition metal (TM) complexes as structure directing agents or building units, three new multinary chalcognidometalates based on T3 supertetrahedral nanocluster of $[Mn_2Ga_4Sn_4S_{20}]^{8-}$ have been solvothermally synthesized and structurally characterized. In compound $Mn_2Ga_4Sn_4S_{20}[Mn_2(en)_5]_2$•$4H_2O$ (**1**, en = ethylenediamine), the neighboring $[Mn_2Ga_4Sn_4S_{20}]^{8-}$ cores were bridged by two pairs of $[Mn_2(en)_5]^{4+}$ complex cations via Mn-S bonds to form one-dimensional (1D) neutral chains. Compound $Mn_2Ga_4Sn_4S_{20}[Mn(dien)_2]_4$•$2H_2O$ (**2**, dien = diethylenetriamine) contains discrete $[Mn_2Ga_4Sn_4S_{20}]^{8-}$ cores separated by $[Mn(dien)_2]^{2+}$ cations. In compound $Mn_2Ga_4Sn_4S_{20}[Mn(teta)]_4$ (**3**, teta = triethylenetetramine), each $[Mn_2Ga_4Sn_4S_{20}]^{8-}$ core was covalently attached by four $[Mn(teta)]^{2+}$ complexes via terminal Mn-S bonds to form a neutral isolated cluster. The photocatalytic experiments indicate that the compound **1** was able to degrade Rhodamine B (RhB) and Crystal Violet (CV) under visible irradiation. Furthermore, the luminescence properties and thermal stabilities of the title compounds as well as the second-order nonlinear optical property of **3** were also studied.

Introduction

13 and 14 main-group metal chalcognidometalates built from supertetrahedral nanoclusters, including supertetrahedron (Tn), pentasupertetrahedron (Pn) and capped supertetrahedron (Cn), have become investigated intensively since the initial report of germanium sulfide cluster of $[Ge_4S_{10}]^{4-}$.[1-5] Among them, Tn clusters with intrinsic well-defined sizes are good candidates for building multifunctional porous materials via covalent interactions. Despite the larger clusters are unlikely to form in pure M^{3+}-Q or M^{4+}-Q (Q = S and Se) compositions, the introduction of mono-valent and divalent transition metal cations are able to effectively enlarge the Tn cluster. Until now, the Tn clusters with different compositions and various sizes such as T2 (e.g. $MnGe_3S_{10}{}^{6-}$), T3 (e.g. $In_{10}S_{20}{}^{10-}$), T4 ($Cd_4In_{16}S_{35}{}^{14-}$) and T5 ($Cd_6In_{28}S_{54}{}^{12-}$) have been characterized.[6-11] By sharing the corner chalcogen atoms, these Tn nanoclusters usually form polymeric structures, especially three-dimensional (3D) porous frameworks with potential applications in photocatalysis, ion exchange and fast ion conductivity, etc.[12]

It should be noted that most of the above chalcognidometalate Tn clusters are charge balanced and space compensated by various protonated organic-amine cations. In recent years, TM complex cations have been widely used as structure-directing reagents, templates or counterions in the syntheses of hybrid chalcognidometalates, especially the unsaturated TM complexes can effectively incorporate the anionic frameworks via TM-Q covalent bonds to form inorganic–organic hybrid chalcognidometalates.[13-16] At the same time, the TM complexes may enhance or improve the electronic, optical and magnetic properties of hybrid chalcognidometalates.[17] For example, Dai and co-worker have reported a series of indium sulfide clusters, namely as Mp-InS (Mp = TM-phen complex and phen=1,10-phenanthroline) and Mb-InS (Mb = TM-bpy complex and bpy = 2,2-bipyridine), in which the discrete T3 and T4 clusters, 1D T3 cluster chains and 2D T3 cluster polymers are separated by $[TM(phen)_3]^{2+}$ and $[TM(bpy)_3]^{2+}$ complex cations, respectively.[18] More interestingly, the isolated T4 clusters and 1D T4 cluster chains can also be bridged by unsaturated $[TM(dach)_2]^{2+}$ (TM = Co, Fe, dach = 1,2-diaminocyclohexane) complex cations to form dimers and 2D structures, respectively.[17-18] Under the direction actions of the different complex cations, these Tn cluster feature remarkable connecting diversities and new structural types.

Among these phases, those containing low-valence metal cations (+1 or +2) and 13 or 14 main group metals are now relatively well-known, however, the limited examples of combining 13 (+3) and 14 (+4) cations are reported partially because that the either cation is apt to form its own chalcognidometalate. Recently, Feng and co-workers explored a series of 13-14-Q (Q = S and Se) phases with protonated amine as cations.[19] Subsequently, $[\{(C_2H_5)_2NH_2\}_2In_2Ge_2S_8]\cdot[(C_2H_5)_2NH]_{0.25}$ and $[C_6H_{14}NO]_{14.4}[Ga_{6.40}Sn_{21.60}S_{52}O_8]$ were also reported.[20] Such combining of different main group cations into one Tn nanocluster also affords another effective strategy to enhance the framework stabilities and tune their physical properties. Intrigued by their rich structural types, we undertook systematic study in the TM complex directed Ga–Sn–S system, about which no phase has been reported until now and only one similar selenide was reported.[19b] Our exploratory studies led to three new manganese gallium tin sulfides, namely, $Mn_2Ga_4Sn_4S_{20}[Mn_2(en)_5]_2\bullet 4H_2O$ (**1**), $Mn_2Ga_4Sn_4S_{20}[Mn(dien)_2]_4\bullet 2H_2O$ (**2**) and $Mn_2Ga_4Sn_4S_{20}[Mn(teta)]_4$ (**3**). They all contain T3 nanocluster of $[Mn_2Ga_4Sn_4S_{20}]^{8-}$ decorated by different Mn-amine complex cations. Herein, we report their syntheses, crystal structures, and physical properties.

Experimental Section

Materials and Instruments. All analytical grade chemicals employed in this study were obtained commercially and used without further purification. Elemental analyses for Mn, Ga, Sn and S were carried out with inductively coupled plasma mass spectrometry (ICP-MS) analysis (Ultima2). C, H and N analyses were performed using a PE2400 II elemental analyzer. The solid-state UV/vis spectra was measured using a computer-controlled PE Lambda 900 UV/vis spectrometer equipped with an integrating sphere in the wavelength range of 200–2500 nm at room temperature. Thermogravimetric analyses (TGA) were carried out with a Mettler TGA/SDTA 851 thermal analyzer under nitrogen atmosphere with a heating rate of 10 ºC min^{-1} in the temperature region of 30-800 ºC.

Syntheses of Compounds 1-3.

$Mn_2Ga_4Sn_4S_{20}[Mn_2(en)_5]_2$•$4H_2O$ (1). A mixture of $Mn(CH_3COO)_2$•$4H_2O$ (2.0 mmol), $Ga(NO_3)_3$•xH_2O (0.5 mmol), $SnCl_2$•$2H_2O$ (0.5 mmol), S (2.8 mmol), en (4.0 mL) and H_2O (1.0 mL) was sealed in a stainless steel reactor with a 15 mL Teflon liner and heated at 180 ºC for 5 days, and then slowly cooled to room temperature. The product consisted of light yellow prismatic crystals of **1** as well as some indefinite dark powders. The crystals were selected by hand and washed with distilled water and ethanol (Yield: 0.097 g, 33% based on Sn). Elemental analyses on grinded single crystals of **1** gave Mn/Ga/Sn/S molar ratios of 3.00(8) : 2.18(2) : 1.89(3) : 9.88(5), which was in good agreement with the result determined by single crystal X-ray diffraction study. C, H and N elemental analyses for $C_{20}N_{20}H_{88}Mn_6Ga_4Sn_4S_{20}O_4$ (**1**), Calcd: C 10.02%, H 3.70%, N 11.68%; Found: C 10.21%, H 3.68%, N 11.98%.

$Mn_2Ga_4Sn_4S_{20}[Mn(dien)_2]_4$•$2H_2O$ (2) and **$Mn_2Ga_4Sn_4S_{20}[Mn(teta)]_4$ (3)**. The compounds **2** and **3** were prepared in the manner analogous to that of **1** except that dien and teta were used instead of en solvent, respectively. Both light yellow crystals of **2** and **3** were filtered, washed by ethanol and air-dried. The yields are 0.048 g (15%) and 0.052 g (18%) on the basis of Ga for **2** and **3**, respectively. Elemental analyses on single crystals of **2** and **3** gave Mn/Ga/Sn/S molar ratios of 3.00(3) : 1.98(3) : 2.12(5) : 10.18(5) and 3.00(6) : 2.11(5) : 2.19(7) : 9.90(3), respectively, which were in good agreement with those determined by single crystal X-ray diffraction study. C, H and N elemental analyses for $C_{32}N_{24}H_{108}Mn_6Ga_4Sn_4S_{20}O_2$ (**2**), Calcd: C 14.86%, H 4.21%, N 13.00%, Found: C 14.75%, H 4.32%, N 13.11%; $C_{24}N_{16}H_{72}Mn_6Ga_4Sn_4S_{20}$ (**3**), Calcd: C 12.48%, H 3.14%, N 9.70%, Found: C 12.34%, H 3.20%, N 9.81%.

Crystal Structure Determination. Single crystals of the title compounds were selected from the reaction products for X-ray crystal diffraction. Data collections for all compounds were performed on a Bruker SMART CCD-based diffractometer (Mo Kα radiation, graphite monochromator) at 293(2) K. Data integrations and cell refinements were done by the INTEGRATE program of the APEX2 software, and multi-scan absorption corrections were applied using the SCALE program for area detector. The structures of the title compounds were solved by using direct method (SHELXTL) and refined by full-matrix least-square technique.[21]

The space groups of the compounds **1-3** were determined to be I222, C2/c and P-4b2, respectively, based on the systematic absences, E-value statistic and satisfactory refinements. In the structural refinements, all the S atoms and Mn amine complexes were easily decided based on their bonding characters and coordination environments, and the metal sites in T3 clusters were initially defined as Ga and Sn atoms based on bond distances, respectively. Such strategy led to final molecules of $Ga_6Sn_4S_{20}[Mn_2(en)_5]_2•4H_2O$, $Ga_6Sn_4S_{20}[Mn(dien)_2]_4•2H_2O$ and $Ga_6Sn_4S_{20}[Mn(teta)]_4$. Obviously, these results were impossible due to the valence imbalance, which is unusual in this series of compounds. Hence, all the Ga sites were finally refined as the statistical mixture of Mn and Ga atoms with free occupation factors, the condition that must be satisfied is $k_{Mn} + k_{Ga} = 1$, where k is the occupancy. Such refinement strategy led to the final chemical molecules of $Mn_2Ga_4Sn_4S_{20}[Mn_2(en)_5]_2•4H_2O$, $Mn_2Ga_4Sn_4S_{20}[Mn(dien)_2]_4•2H_2O$ and $Mn_2Ga_4Sn_4S_{20}[Mn(teta)]_4$, respectively, which were also proved by the inductively coupled plasma mass spectrometry (ICP-MS) analyses. Non-hydrogen atoms were refined with anisotropic displacement parameters, and the hydrogen atoms bonded to C, N and O atoms were located at geometrically calculated positions. Data collection and refinement parameters for all the compounds are summarized in Table 1. Important bond lengths are listed in Table 2. More details on the crystallographic studies are given in Supporting Information.

Powder X-ray Diffraction. The powder X-ray Diffraction (PXRD) patterns of the ground powder of **1-3** were collected at room temperature on a X'Pert-Pro diffractometer using Cu Kα radiation (λ = 1.5406 Å) in the 2θ range of 5–80º. PXRD patterns are in good agreement with the simulated patterns generated using the CIF documents of each refined structure (Fig. S6). The relative big lump at small 2θ angles mainly originated from the excessively small amount of experimental sample. Furthermore, weak crystal quality and relative larger particle sizes of powder also decreased the measurement accuracies. But this did not affect the results of subsequent physical properties.

Photoluminescence Measurement. The solid-state luminescence emission spectra were recorded on a FLS920 fluorescence spectrophotometer equipped (Edinburgh Instruments Ltd.) with a continuous Xe-900 xenon lamp and a μF900 microsecond flash lamp.

SHG Measurements. Measurement of the powder frequency-doubling effect was carried out on the sieved sample (70-100 mesh) by means of the modified method of Kurtz and Perry. The fundament wavelength is 1064 nm generated by a Q-switched Nd:YAG laser. Sieved KDP (KH_2PO_4) sample in the same size range was used as a reference.

Photocatalytic Activity Measurements. The photocatalytic activities of as-prepared samples were evaluated by the degradation of Rhodamine B (RhB) and Crystal Violet (CV) under visible light irradiation of a 500 W Xe lamp. The cut-off filter was used to remove all wavelengths less than 400 nm and more than 780 nm ensuring irradiation with visible-light only. In the typical process, 25 mg of sample as photocatalyst was added into 50 mL of RhB and CV solution (10 mg/L), respectively. After being dispersed in an ultrasonic bath for 30 min, the solution was stirred for 2 h in the dark before irradiation to reach adsorption equilibrium between the catalyst and solution, and then was exposed to visible light irradiation. About 4 mL suspension was continually taken from the reaction cell and collected by centrifugation at 120 and 30 min intervals during the irradiation for RhB and CV, respectively. The resulting solution was analyzed on a GBC Cintra 2020 UV/Vis spectrophotometer.

Results and Discussion

TM complex cations have been widely used in the syntheses of inorganic–organic hybrid chalcognidometalates because of their excellent templates or structure-directing effects. In this paper, we adopt bi- and tri- and tetra-dentate chelating amines of en, dien and teta in situ coordinated to Mn^{2+} ions leading to three different types of TM complexes, which induce three new Mn-Ga-Sn-S phases with diversified structures from 0D cluster to 1D chains based on $[Mn_2Ga_4Sn_4S_{20}]^{8-}$ T3 supertetrahedral clusters.

Crystal Structures

$Mn_2Ga_4Sn_4S_{20}[Mn_2(en)_5]_2{\cdot}4H_2O$ (1). Compound **1** crystallizes in the orthorhombic system ($I222$) and features a 1D neutral chain based on $[Mn_2Ga_4Sn_4S_{20}]^{8-}$ T3 supertetrahedral cluster interlinked by $[Mn_2(en)_5]^{4+}$ complexes via Mn-S bonds. In the $[Mn_2Ga_4Sn_4S_{20}]^{8-}$ cluster, there are one crystallographically independent Sn^{4+}, there M (M = Mn/Ga) sites and five S^{2-} ions. All the Sn^{4+} cations occupy the four corners of T3 cluster with slightly longer Sn-S bond distances of 2.3489(16)-2.4039(14) Å, which are in accordance with those of $[SnS_4]$ tetrahedra in Ga-Sn-S phases as well as thiostannates.[18,22] The other six core sites of T3 cluster are occupied by two M(1), two M(2) and two M(3) metals with tetrahedral environments, which are supported by the corresponding interatomic distances. For example, the M-S bonds fall into the medium distances range of 2.2797(15)-2.3699(15) Å, which are slightly longer than the sole Ga-S pairs in reported gallium sulfide clusters, but shorter than the typical Mn-S bonds of $[MnS_4]$ tetrahedra in $(1,4\text{-dabH})_2MnSnS_4$, etc.[23] Furthermore, the M(1)-S and M(2)-S lengths fall in the range of 2.3073(18)-2.3499(15) Å and 2.3310(19)-2.3699(15) Å, respectively, whereas the M(3)-S bonds feature slightly shorter distances of 2.2797(15)-2.3066(14) Å. These slightly differences originate from the different Mn/Ga ratios, that is, the less Mn content in M(3) site leads to shorter M-S lengths and more Mn contents of M(1) and M(2) sites result in longer M-S lengths. Using Brown's bond-valence model, the calculated valence sums surrounding the M(1), M(2) and M(3) sites are 2.46, 2.61 and 2.87, respectively, which are also in good agreement with the refinement results.[24]

The $Mn(4)^{2+}$ ion is coordinated by four nitrogen donors from two chelate en ligands to form a $[Mn(en)_2]^{2+}$ complex, which has been reported in many chalcognidometalate.[25] Such two neighboring complexes are further bridged by a chain-like en ligand via Mn-N bonds to form a $[Mn_2(en)_5]^{4+}$ complex cation. Similar $[Mn_2(en)_5]^{4+}$ complex cation was reported in $[Mn(en)_3]\{[Mn(en)_2]_2[Mn_2(en)_5](SbSe_4)_4{\cdot}2H_2O$.[26] The neighboring $[Mn_2Ga_4Sn_4S_{20}]^{8-}$ T3 supertetrahedral cores are interlinked by two pairs of $[Mn_2(en)_5]^{4+}$ complexes via Mn-S bonds to form a 1D neutral $Mn_2Ga_4Sn_4S_{20}[Mn_2(en)_5]_2$ chain along the a-axis (Fig. 2a). Hence, the $Mn(4)^{2+}$ ion is coordinated by five N atoms and one terminal S atom from T3 cluster with an octahedral environment. Each 1D $Mn_2Ga_4Sn_4S_{20}[Mn_2(en)_5]_2$ chain interact with four neighboring chains via weak N-H···S hydrogen bonds resulting in a 3D H-bonding network with 1D large tunnels along the a-axis, which are located by dissociative H_2O molecules (Fig. 2b). Such 1D channel has a nearly quadrangular cross-section of 5.86 × 11.02 $Å^2$ presented in the framework along the a-axis. The N···S distances (3.359(7)-3.627(8) Å) and N-H···S angles (143.1-170.2°) are in accordance with the values reported in the literatures.[27]

$Mn_2Ga_4Sn_4S_{20}[Mn(dien)_2]_4$•$2H_2O$ (2) Compound **2** crystallizes in the monoclinic space group C2/c (No. 15) and contains discrete $[Mn_2Ga_4Sn_4S_{20}]^{8-}$ T3 supertetrahedral clusters separated and charge balanced by $[Mn(dien)_2]^{2+}$ complex cations (Fig. 3). In the $[Mn_2Ga_4Sn_4S_{20}]^{8-}$ cluster of **2**, the Sn^{4+} cations also occupy the four corners and all the M metals are located at the core sites, which is similar to that of **1**. Differently, the T3 cluster of **2** is composed of two crystallographically independent Sn^{4+} and four M metals. Two Sn(1) and two Sn(2) cations occupy the four corners of T3 cluster with Sn-S bond distances of 2.3220(11)-2.4222(9) Å, which are close to those of **1**. Two M(1), two M(2), one M(3) and one M(4) atoms occupy the core metal sites with M-S bond lengths of 2.2640(9)-2.4117(9) Å, which also features evidently consistency with the ratios of Mn/Ga content. The M(1) site is mostly occupied by Mn element (k_{Mn} = 0.71) and feature longer M-S distances of 2.3686(10)-2.4155(9) Å, and the M(2), M(3) sites feature less Mn content (k_{Mn} = 0.17) with medium lengths of 2.2640(9)-2.3123(8) Å, whereas the M(4) site is almost occupied by Ga element (k_{Mn} = 0.08) with shortest distances of 2.2646(9)-2.2984(8) Å. These bond distances further prove the co-occupation of Mn and Ga elements in the T3 cluster. The calculated valence sums surrounding M(1), M(2), M(3) and M(4) sites are 2.1, 2.8, 2.8 and 2.9, respectively, which are also in good agreement with the above results.

The neighboring $[Mn_2Ga_4Sn_4S_{20}]^{8-}$ T3 cluster are interconnected by two types of $[Mn(5)(dien)_2]^{2+}$ and $[Mn(6)(dien)_2]^{2+}$ complex cations via weak intercluster N-H···S hydrogen bonds resulting in a layered arrangement parallel to the bc-plane, which are further packed into a 3D network with A···A···A sequence along the a-axis through N-H···S hydrogen bonds (Fig. 3). The N···S distances (3.217(12)-3.771(6) Å) and N-H···S angles (132.3-166.0º) are accordance with the values in compound **1**.

$Mn_2Ga_4Sn_4S_{20}$[Mn(teta)]$_4$ (3). The crystal structural analysis revealed that the compound **3** crystallizes in noncentrosymmetric space group P-4b2. As shown in Fig. 4, its structure is isotypical to [Mn(tepa)]$_4$[$Zn_2Ga_4Sn_4Se_{20}$] with [Mn(tepa)]$^{2+}$ complex replaced by [Mn(teta)]$^{2+}$ and [$Zn_2Ga_4Sn_4Se_{20}$]$^{8-}$ core substituted by [$Mn_2Ga_4Sn_4S_{20}$]$^{8-}$ cluster, respectively.[20] Its structure features a neutral isolated molecular cluster built from one T3 supertetrahedral core covalently attached by four [Mn(teta)]$^{2+}$ complexes via terminal Mn-S bonds.

The T3 cluster of **3** is consisted of two M metals and one Sn^{4+} cation, which is different from those of **1** and **2**. The Sn-S bond distances are of 2.3649(12)-2.3806(12) Å, and the M-S bond lengths fall into the medium distances range of 2.2692(12)-2.3441(11) Å, which are close to those of **1** and **2**. The calculated valence sums surrounding both M(1) and M(2) sites of 2.7 are in good agreement with the refiment results (k_{Mn} = 0.33). In the [Mn(teta)]$^{2+}$ complex cation, the Mn^{2+} ion is coordinated by four N atoms from one teta ligand and one S^{2-} ion from the T3 cluster showing a distorted tetragonal pyramidal environment. Each centered [$Mn_2Ga_4Sn_4S_{20}$]$^{8-}$ T3 cluster is terminally attached by four [Mn(teta)]$^{2+}$ complex cations via Mn-S bonds to form a neutral [$Mn_2Ga_4Sn_4S_{20}$][Mn(teta)]$_4$ molecular nanocluster. Each neutral cluster interacts with neighboring ones via weak intercluster N-H···S hydrogen bonds resulting in a layered arrangement parallel to the ab-plane. The layered structure further pack into a 3D network in A···A···A order along the c-axis through the N-H···S hydrogen bonds (Fig. 4).

Optical and Luminescence Properties The solid-state optical diffuse reflection spectra of the compounds **1-3** were measured at room temperature. The absorption (α/S) data were calculated from the reflectance using the Kubelka-Munk function. As shown in Fig. 5, the optical band gaps of **1-3** obtained by extrapolating the linear portion of the absorption edge are estimated as 2.75, 2.66 and 2.82 eV, respectively, which are in accordance with their light yellow colors. Obviously, the title compounds exhibit red shift of the absorption edge compared with the bulk Ga_2S_3 (3.3 eV), and similar red shift has been found in other inorganic–organic hybrid chalcogenidogallates, such as UCR-19ZnGaS-Teta (2.60 eV), $[Cu_2Ga_{16}Sn_2S_{35}]\cdot12(C_5NH_{12})$ (2.11 eV) and UCR-7GaS-DBA (2.84 eV, DBA=di-n-butylamine), etc.[28] Comparing with the bulk SnS_2 (2.44 eV), there are blue shift of the absorption edges of the title compounds, which is similar to those of $(1,4\text{-dabH})_2MnSnS_4$ (2.9 eV) and $[Ni(C_8N_5H_{23})]_2Sn_2S_6$ (2.8 eV), etc.[23c,29] Further, these hybrid materials feature slightly different band gaps mainly due to the different coordination environments of Mn^{2+} ions as well as the distinct connecting manners between the $[Mn_2Ga_4Sn_4S_{20}]^{8-}$ cluster and complex cations. Hence, it demonstrates the possibility to tune the band gaps of hybrid chalogenides by combing different chelating amines into crystals.

All the title compounds exhibit strongly luminescent properties with broad emission by irradiation of UV light (λ = 355 nm) (Fig. S4). Compound **1** gives pronounced purple emission with λ_{max} = 430 nm. Besides this comparably stronger emission, one shoulder peak is also found at about 479 nm with blue color. Compounds **2** and **3** exhibit similar purple emission with λ_{max} = 395 nm. These luminescent properties are similar to those found for microporous Ga-Sn-S materials (460-508 nm).[18a]

Compound **3** crystallizes in the noncentrosymmetric space group of P-4b2 (No. 117), hence, its second-order nonlinear optical effect was investigated. Fig. S5 shows the curve of the SHG signal intensity for ground crystal of **3**. The result indicates that compound **3** exhibits a SHG efficiency of about 1/6 × KDP (KDP: the comparison was performed with similar particle sizes). Given that the centrosymmetric structure of $[Mn_2Ga_4Sn_4S_{20}]^{8-}$ T3 cluster, the very weak NLO behavior of **3** should originates from the noncentrosymmetric packing mode of the T3 clusters.

Thermal Stabilities The thermal stabilities of **1-3** were examined by thermogravimetric analyses (TGA) in N_2 atmosphere from 30 to 800 ºC (Fig. 6). The TGA curves show that the compounds **1** and **2** both feature lower stabilities under heating condition. Compound **1** starts to decompose at 30 °C and continue loses weight up to 420 °C with a final weight loss of 27.8 %, corresponding to the release of all en ligands and H_2O molecules (calcd. 27.1%). Compound **2** also features consecutive decomposition from 30 °C to

450 °C with total weight loss of 33.4%, which is close to the calculated amount (33.3 %) of all dien ligands and H_2O molecules. Differently, compound **3** is able to stable up to 300 °C, and then the TGA curve displays one main step of weight loss from 300 °C to 400 °C, which corresponds to the loss of all teta ligands. The observed weight loss of 24.7 % is close to the theoretical value of 25.3%.

Photocatalytic Properties. The photocatalytic activity of the compound **1** was evaluated by the degradation of RhB and CV under visible light irradiation at room temperature as the test pollutant. Temporal changes in the concentration of RhB and CV were monitored by examining the variations of intensities in the maximal absorption in UV-Vis spectra at 554 and 535 nm, respectively. The degradation efficiencies are defined as C/C_0, where C and C_0 represent the remnant and initial concentration of RhB and CV, respectively. Fig. 7 illustrates the time dependent absorption spectra of RhB and CV. For RhB, compound **1** features lower photocatalytic effect, and the degradation ratio of RhB reached 80% exposed to visible light for 6 hours, and achieved nearly 100% after 10 hours, resulting in complete decolorization. Such phenomena is also demonstrated by the change in the color of the dispersion from an initial red to a nearly colorless (the inset of Fig. 7a). Interestingly, compound **1** shows high effective photocatalytic activity for CV, and the degradation ratio of CV reached 100% exposed to visible light for 1.5 hours, resulting in complete decolorization. The results demonstrate that compound **1** displays selectively photocatalytic ability under visible light irradiation. The XRD characterizations show that there is no change before and after the photocatalytic process, demonstrating the stability of compound **1** as the photocatalyst (Fig. S3).

Conclusions

In conclusion, a series of new inorganic–organic hybrid manganese gallium tin sulfides based on $[Mn_2Ga_4Sn_4S_{20}]^{8-}$ T3 nanoclusters have been solvothermally synthesized, structurally, optically and thermally characterized. It is most fascinating features of these compounds that the TM complexes not only afford as charge balances but also covalently bridge the T3 clusters to form neutral inorganic–organic hybrid chalcognidometalates. The successful syntheses of the title compounds provide possibilities of constructing new open-framework chalcogenidometalates based on Tn supertetrahedral clusters and unsaturated metal complexes via strong covalent bonding action. The photocatalytic experiments show our materials have the selective photodegradative abilities to degrade different organic contaminant, demonstrating the photochemical properties of the inorganic–organic hybrid chalcognidometalates. Research on this subject is in progress.

Acknowledgments

We thank the financial supports from the National Nature Science Foundation of China (Nos. 21101075 and 21201081).

Supplementary Information

Electronic supplementary information (ESI) available: Crystallographic data in CIF format (CCDC numbers 1013845 for **1**, 1013846 for **2** and 1013847 for **3**), tables of hydrogen bonds, photoluminescent emission spectra, and powder XRD patterns for all compounds as well as oscilloscope trace of SHG signal for **3**.

REFERENCES

1. (a) H. Li, A. Laine, M. O'Keeffe and O. M. Yaghi, Science., 1999, **283**, 1145; (b) H.-L. Li, J. Kim, T. L. Groy and M. O'Keeffe, O. M. Yaghi, J. Am. Chem. Soc., 2001, **123**, 4867; (c) C. Wang, X. H. Bu, N. F. Zheng and P. Y. Feng, J. Am. Chem. Soc., 2002, **124**, 10268.
2. (a) N. F. Zheng, X. H. Bu and P. Y. Feng, Nature., 2003, **426**, 428; (b) X. H. Bu, N. F. Zheng and P. Y. Feng, Chem. Eur. J., 2004, **10**, 3356; (c) P. Y. Feng, X. H. Bu and N. F. Zheng, Acc. Chem. Res., 2005,

38, 293.

3. (a) J. Zhou, J. Dai, G. Q. Bian and C. Y. Li, Coord. Chem. Rev., 2009, **253**, 1221; (b) P. Vaqueiro and M. L. Romero, Inorg. Chem., 2009, **48**, 810; (c) Q. C. Zhang, T. Wu, X. H. Bu, T. Tran and P. Y. Feng, Chem. Mater., 2008, **20**, 4170; (d) H. L. Li, J. Kim, M. O'Keeffe and O. M. Yaghi, J. Am. Chem. Soc. 2003, **42**, 1819; (e) Q. P. Lin, X. H. Bu and P. Y. Feng, Chem. Commun., 2014, **50**, 4044.

4 (a) N. F. Zheng, X. H. Bu and P. Y. Feng, J. Am. Chem. Soc., 2003, **125**, 1138; (b) C. L. Cahill and J. B. Parise, Dalton Trans., 2000, 1475; (c) N. Hüsing, Angew. Chem. Int. Ed., 2008, **47**, 1992.

5. (a) S. Bag, P. N. Trikalitis, P. J. Chupas, G. S. Armatas, M. G. Kanatzidis, Science., 2007, **317**, 490; (b) Y. M. Lin,W. Massa and S. Dehnen, Chem. Eur. J., 2012, **18**, 13427; (c) Y. M. Lin, W. Massa and S. Dehnen, J. Am. Chem. Soc., 2012, **134**, 4497; (d) F. L. Hu, J. Zhou, X. Liu, R. Chen, W. S. Fu and Y. C. Wei, Cryst. Eng. Comm., 2013, **15**, 1194; (e) M. Ribes, J. Oliver-Fourcade, E. Philippot and M. Maurin, J. Solid State Chem., 1973, **8**, 195.

6. (a) Z. Q. Wang, G. F. Xu, Y. F. Bi and C. Wang, Cryst. Eng. Comm., 2010, **12**, 3703; (b) D. Pitzschke, C. Näther and W. Bensch, Solid State Sci., 2002, **4**, 1167; (c) H. L. Li, J. Kim, T. L. Groy, M. O'Keeffe and O. M. Yaghi, J. Am. Chem. Soc., 2001, **123**, 4867; (d) W. P. Su, X. Y. Huang, J. Li and H. X. Fu, J. Am. Chem. Soc. 2002, **124**, 12944.

7. (a) L. Wang, T. Wu, X. H. Bu, X. Zhao, F. Zuo and P. Y. Feng, Inorg. Chem., 2013, **52**, 2259; (b) J. Lin, Q. Zhang, L. Wang, X. C. Liu, W. B. Yan, T. Wu, X. H. Bu and P. Y. Feng, J. Am. Chem. Soc., 2014, **136**, 4769.

8. (a) N. F. Zheng, X. H. Bu and P. Y.Feng, Angew. Chem. Int. Ed., 2004, **43**, 4753; (b) Y. H. Wang, W. Luo, J. B. Jiang, G. Q. Bian, Q. Y. Zhu and J. Dai, Inorg. Chem., 2012, **51**, 1219.

9. (a) T. Wu, Q. Zhang, Y. Hou, L. Wang, C. Y. Mao, S. T. Zheng, X. H. Bu and P. Y. Feng, J. Am. Chem. Soc., 2013, **135**, 10250; (b) W. W. Xiong, J. R. Li, B. Hu, B. Tan, R. F. Li and X. Y. Huang, Chem. Sci., 2012, **3**, 1200; (c) T. Wu, X. H. Bu, P. H. Liao, L. Wang, S. T. Zheng, R. Ma and P. Y. Feng, J. Am. Chem. Soc., 2012, **134**, 3619; (d) T. Wu, R. Khazhakyan, L. Wang, X. H. Bu, S. T. Zheng, V. Chau and P. Y. Feng, Angew. Chem. Int. Ed., 2011, **50**, 2536.

10. (a) T. Wu, F. Zuo, L. Wang, X. H. Bu, S. T. Zheng, R. Ma and P. Y. Feng, J. Am. Chem. Soc., 2011, **133**, 15886; (b) P. Vaqueiro, M. L. Romero, B. C. Rowan and B. S. Richards, Chem. Eur. J., 2010, **16**, 4462; (c) L. Wang, T. Wu, F. Zuo, X. Zhao, X. H. Bu, J. Z. Wu and P. Y. Feng, J. Am. Chem. Soc., 2010, **132**, 3283.

11. (a) P. Vaqueiro, Inorg. Chem., 2008, **47**, 20; (b) M. J. Manos, C. D. Malliakas and M. G. Kanatzidis, Chem. Eur. J., 2007, **13**, 51.

12 (a) N. F. Zheng, X. H. Bu and P. Y. Feng, Nature., 2003, **426**, 428; (b) N. F. Zheng, X. H. Bu, H. Vu and P. Y. Feng, Angew. Chem. Int. Ed., 2005, **44**, 5299; (c) M. J. Manos, R. G. Iyer, Eric Quarez, J. H. Liao and M. G. Kanatzidis, Angew. Chem. Int. Ed., 2005, **44**, 3552; (d) M. J. Manos, C. D. Malliakas and M. G. Kanatzidis, Chem. Eur. J., 2007, **13**, 51.

13 (a) G. N. Liu, J. D. Lin, Z. N. Xu, Z. F. Liu, G. C. Guo and J. S. Huang, Cryst. Growth Des., 2011, **11**, 3318; (b) G. N. Liu, G. C. Guo, F. Chen, S. H. Wang, J. Sun and J. S. Huang, Inorg. Chem., 2012, **51**, 472; (c) G. N. Liu, X. M. Jiang, M. F. Wu, G. E. Wang, G. C. Guo and J. S. Huang, Inorg. Chem., 2011, **50**, 5740; (d) B. Seidlhofer, C. Näther and W. Bensch, Cryst. Eng. Comm., 2012, **14**, 5441.

14 (a) B. Seidlhofer, J. Djamil, C. Näther and W. Bensch, Cryst. Growth Des., 2011, **11**, 5554; (b) C. Y. Yue, X. W. Lei, H. P. Zang, L. J. Feng, J. Q. Zhao and X. Y. Liu, Cryst. Eng. Comm., 2014, **16**, 3424; (c) Y. H. Liu, S. H. Porter and J. E. Goldberger, J. Am. Chem. Soc., 2012, **134**, 5044.

15 (a) J. Zhou, X. H. Yin and F. Zhang, Inorg. Chem., 2010, **49**, 9671; (b) J. Zhou, L. T. An and F. Zhang, Inorg. Chem., 2011, **50**, 415; (c) M. Zhang, T. L. Sheng, X. Wang, S. M. Hu, R. B. Fu, J. S. Chen, Y. M. He, Z. T. Qin, C. J. Shen and X. T. Wu, Cryst. Eng. Comm., 2010, **12**, 73.

16 (a) Z. Q. Wang, H. J. Zhang and C. Wang, Inorg. Chem., 2009, **48**, 8180; (b) Z. Q. Wang, G. F. Xu, Y. F. Bi and C. Wang, Cryst. Eng. Comm., 2010, **12**, 3703. (c) C. Y. Yue, X. W. Lei, Y. X. Ma, N. Sheng, Y. D. Yang, G. D. Liu and X. R. Zhai, Cryst. Growth Des., 2014, **14**, 101.

17. (a) K. Z. Du, M. L. Feng, L. H. Li, B. Hu, Z. J. Ma, P. Wang, J. R. Li, Y. L. Wang, G. D. Zou and X. Y. Huang, Inorg. Chem., 2012, **51**, 3926-3928. (b) Y. P. Zhang, X. Zhang, W. Q. Mu, W. Luo, G. Q.

Bian, Q. Y. Zhu and J. Dai, Dalton Trans., 2011, **40**, 9746. (c) G. N. Liu, G. C. Guo, F. Chen, S. P. Guo, X. M. Jiang, C. Yang, M. S. Wang, M. F. Wu and J. S. Huang, Cryst. Eng. Comm., 2010, **12**, 4035-4037.

18 (a) Z. X. Lei, Q. Y. Zhu, X. Zhang, W. Luo, W. Q. Mu and J. Dai, Inorg. Chem., 2010, **49**, 4385; (b) X. Zhang, W. Luo, Y. P. Zhang, J. B. Jiang, Q. Y. Zhu and J. Dai, Inorg. Chem., 2011, **50**, 6972; (c) Y. Y. Pu, X. Zhang, L. S. You, G. Q. Bian, Q. Y. Zhu and J. Dai, Z. Anorg. Allg. Chem., 2012, **638**, 2498; (d) J. Zhou, Y. Zhang, G. Q. Bian, C. Y. Li, X. X. Chen and J. Dai, Cryst. Growth Des., 2008, **7**, 2235; (e) Y. H. Wang, M. H. Zhang, Y. M. Yan, G. Q. Bian, Q. Y. Zhu and J. Dai, Inorg. Chem., 2010, **49**, 9731.

19 (a) N. F. Zheng, X. H. Bu, B. Wang and P. Y. Feng, Science., 2002, **298**, 2366; (b) G. H. Xu, P. Guo, S. Y. Song, H. J. Zhong and C. Wang, Inorg. Chem., 2009, **48**, 4628.

20 (a) D. Pitzschke and W. Bensch, Z. Anorg. Allg. Chem., 2003, **629**, 2206. (b) X. H. Han, Z. Q. Wang, D. Liu, J. Xu, Y. X. Liu and C. Wang, Chem. Commun., 2014, **50**, 796.

21 G. M. Sheldrick, SHELXTL, University of Götingen, Götingen, 2001.

22 (a) M. Behrens, M.-E. Ordolff, C. Näther, W. Bensch, K.-D. Becker, C. Guillot-Deudon, A. Lafond and J. A. Cody, Inorg. Chem., 2010, **49**, 8305; (b) R. C. Zhang, H. G. Yao, S. H. Ji, M. C. Liu, M. Jia and Y. L. An. Chem. Commun., 2010, **46**, 4550; (c) W. W. Xiong, G. D. Zhang and Q. C. Zhang, Inorg. Chem. Front., 2014, **1**, 292; (d) W. W. Xiong, J. W. Miao, P. Z. Li, Y. L. Zhao, B. Liu and Q. C. Zhang, Cryst. Eng. Comm., 2014, **16**, 5989.

23 (a) H. Lin, L. J. Zhou and L. Chen, Chem. Mater., 2012, **24**, 3406; (b) K. Feng, Y. G. Shi, W. L. Yin, W. D. Wang, J. Y. Yao and Y. C. Wu, Inorg. Chem., 2012, **51**, 11144; (c) N. Pienack, K. Möller, C. Näther and W. Bensch, Solid State Sci., 2007, **9**, 1110; (d) J. Hilbert, C. Näther and W. Bensch, Inorg. Chem., 2014, **53**, 5619.

24 D. Altermatt, I. D. Brown, Acta Crystallogr., 1985, **B41**, 240.

25 (a) M. L. Fu, G. C. Guo, L. Z. Cai, Z. J. Zhang and J. S. Huang, Inorg.Chem., 2005, **44**, 184; (b) X. M.

Gu, J. Dai, D. X. Jia, Y. Zhang and Q. Y. Zhu, Cryst.Growth Des., 2005, **5**, 1845; (c) P. Vaqueiro, Inorg.Chem., 2006, **45**, 4150; (d) Z. Q. Wang, G. F. Xu, Y. F. Bi and C. Wang, Cryst. Eng. Comm., 2010, **12**, 3703.

26 W. Bensch, C. Näther and M. Schur, Chem. Commun., 1997, 1773.

27 (a) C. Y. Yue, Z. D. Yuan, L. G. Zhang, Y. B. Wang, G. D. Liu, L. K. Gong and X. W. Lei, J. Solid State Chem., 2013, **206**, 129; (b) C. Y. Yue, X. W. Lei, R. Q. Liu, H. P. Zhang, X. R. Zhai, W. P. Li, M. Zhou, Z. F. Zhao, Y. X. Ma and Y. D.Yang, Cryst. Growth Des., 2014, **14**, 2411.

28 (a) X. H. Bu, N. F. Zheng, X. Q. Wang, B. Wang and P. Y. Feng, Angew. Chem. Int. Ed., 2004, **43**, 1502; (b) T. Wu, X. H. Bu, V. Chau and P. Y. Feng, J. Am. Chem. Soc., **132**, 10823.

29 N. Pienack, S. Lehmann, H. Lühmann, M. El-Madani, C. Näther and W. Bensch, Z. Anorg. Allg. Chem. 2008, **634**, 2323.

Table 1. Crystal Data and Structure Refinements for Compounds **1- 3**

Compound	**1**	**2**	**3**
chemical formula	$C_{20}N_{20}H_{88}Mn_6Ga_4Sn_4S_{20}O_4$	$C_{32}N_{24}H_{108}Mn_6Ga_4Sn_4S_{20}O_2$	$C_{24}N_{16}H_{72}Mn_6Ga_4Sn_4S_{20}$
fw	2397.58	2585.90	2309.57
Space group	I222 (No. 23)	C2/c (No. 15)	P-4b2 (No. 117)
a/Å	10.9793(18)	27.616(2)	16.569(5)
b/Å	16.526(3)	13.5823(11)	16.569(5)
c/Å	22.757(4)	26.546(3)	12.637(4)
β/º	90	119.1350(10)	90
V(Å^3)	4129.1(11)	8697.1(15)	3469.1(17)
Z	2	4	2
D_{calcd} (g cm^{-3})	1.928	1.975	2.211
Temp (K)	293(2)	293(2)	293(2)
μ (mm^{-1})	3.891	3.706	4.626
F(000)	2316	5112	2244
Reflections	24211	49875	38945
Unique	4742	9996	3957
Reflections	4063	8036	3631
GOF on F^2	1.012	1.027	1.048
R1,wR2 (I > 2σ(I))[a]	0.0327/0.0900	0.0323/0.0783	0.0228/0.0535
R1,wR2 (all data)	0.0437/0.0972	0.0457/0.0855	0.0273/0.0555
$\Delta\rho_{max}$ (e/Å^3)	1.433	1.958	0.822
$\Delta\rho_{min}$ (e/Å^3)	-0.417	-0.810	-0.321

[a] $R1 = \sum||F_o| - |F_c||/\sum|F_o|$, $wR2 = \{\sum w[(F_o)^2 - (F_c)^2]^2/\sum w[(F_o)^2]^2\}^{1/2}$

Table 2. Selected Bond Lengths (Å) for Compounds **1-3**.

		1	
Mn(4)-N(3)	2.251(5)	Mn(4)-N(4)	2.296(5)
Mn(4)-N(5)	2.279(5)	Mn(4)-N(2)	2.317(6)
Mn(4)-N(1)	2.283(5)	Mn(4)-S(5)	2.5936(18)
Sn(1)-S(5)	2.3489(15)	M(2)-S(3)#2	2.3314(18)
Sn(1)-S(4)	2.3955(17)	M(2)-S(3)#1	2.3314(18)
Sn(1)-S(3)	2.3972(16)	M(2)-S(1)	2.3697(14)
Sn(1)-S(2)	2.4037(14)	M(2)-S(1)#3	2.3697(14)
M(1)-S(4)	2.3073(18)	M(3)-S(2)#1	2.2800(14)
M(1)-S(4)#2	2.3073(18)	M(3)-S(2)	2.2800(14)
M(1)-S(1)#2	2.3497(14)	M(3)-S(1)#1	2.3065(14)
M(1)-S(1)	2.3498(14)	M(3)-S(1)	2.3065(14)
		2	
Mn(6)-N(3)	2.248(3)	Mn(5)-N(9)	2.261(2)
Mn(6)-N(4)	2.279(2)	Mn(5)-N(11)	2.2690(19)
Mn(6)-N(6)	2.299(2)	Mn(5)-N(7)	2.285(2)
Mn(6)-N(2)	2.302(2)	Mn(5)-N(12)	2.284(2)
Mn(6)-N(5)	2.319(3)	Mn(5)-N(10)	2.287(2)
Mn(6)-N(1)	2.331(3)	Mn(5)-N(8)	2.311(2)
Sn(1)-S(3)	2.3228(6)	Sn(2)-S(1)	2.3225(9)
Sn(1)-S(5)	2.3901(7)	Sn(2)-S(2)	2.3825(7)
Sn(1)-S(8)	2.4174(7)	Sn(2)-S(7)	2.4132(5)
Sn(1)-S(6)	2.4222(5)	Sn(2)-S(4)	2.4213(7)
M(1)-S(5)	2.3695(6)	M(3)-S(6)#1	2.2639(6)
M(1)-S(2)#1	2.3912(8)	M(3)-S(6)	2.2640(6)
M(1)-S(9)#1	2.4118(5)	M(3)-S(9)	2.3018(6)
M(1)-S(10)	2.4155(6)	M(3)-S(9)#1	2.3018(6)
M(2)-S(7)	2.2736(7)	M(4)-S(4)#1	2.2648(7)
M(2)-S(8)	2.2785(6)	M(4)-S(4)	2.2648(7)
M(2)-S(9)	2.3088(5)	M(4)-S(10)#1	2.2982(5)
M(2)-S(10)	2.3123(6)	M(4)-S(10)	2.2982(5)
		3	
Mn(3)-N(3)	2.150(5)	Mn(3)-N(4)	2.228(4)
Mn(3)-N(1)	2.208(4)	Mn(3)-N(2)	2.265(5)
		Mn(3)-S(1)	2.3871(14)

Sn(1)-S(2)	2.3660(12)	M(1)-S(4)	2.2859(12)
Sn(1)-S(1)	2.3672(11)	M(1)-S(3)#2	2.3018(12)
Sn(1)-S(4)	2.3765(12)	M(1)-S(5)#3	2.3375(11)
Sn(1)-S(3)	2.3796(11)	M(1)-S(5)	2.3449(11)
M(2)-S(2)	2.2695(12)	M(2)-S(5)	2.3328(10)
M(2)-S(2)#1	2.2695(12)	M(2)-S(5)#1	2.3328(10)

M = Ga/Mn, Symmetric codes: for **1** #1 x, -y, -z #2 -x+1, -y, z #3 -x+1, y, -z; for **2** #1 -x, y, -z+1/2; for **3** #1 -x, -y, z #2 y, -x, -z+1 #3 -y, x, -z+1.

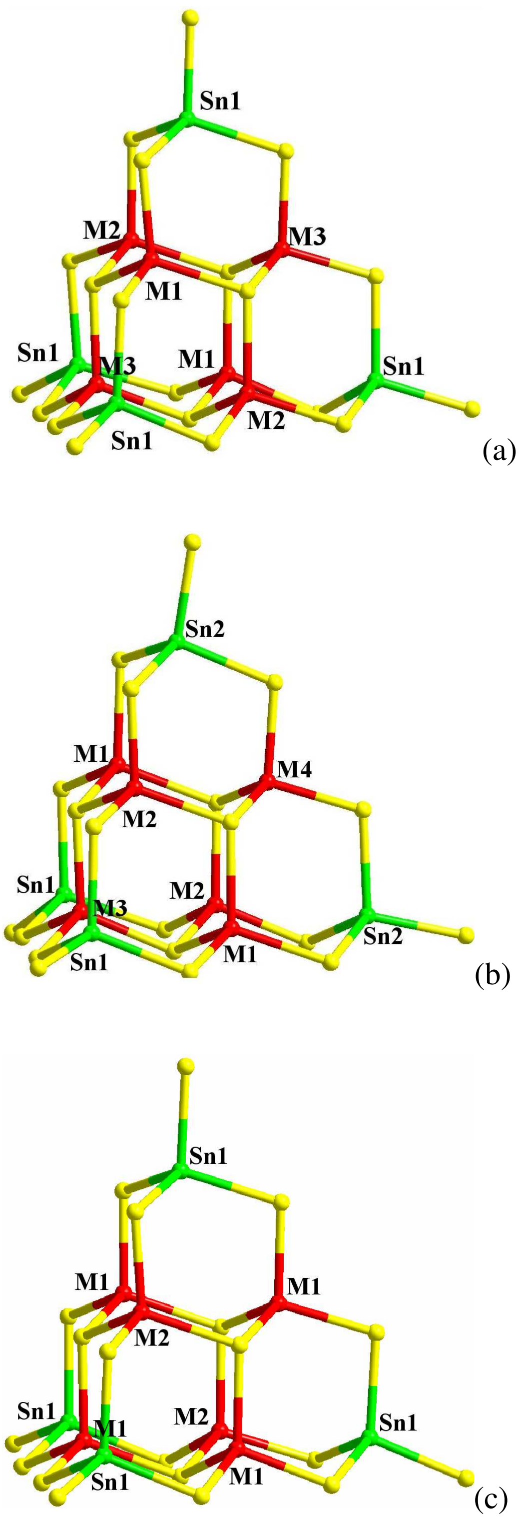

Fig. 1. General View of the $[Mn_2Ga_4Sn_4S_{20}]^{8-}$ T3 supertetrahedral nanocluster in Compounds **1**, **2** and **3** (a-c). The M (M = Mn/Ga), Sn and S atoms are drawn as red, green and yellow spheres, respectively.

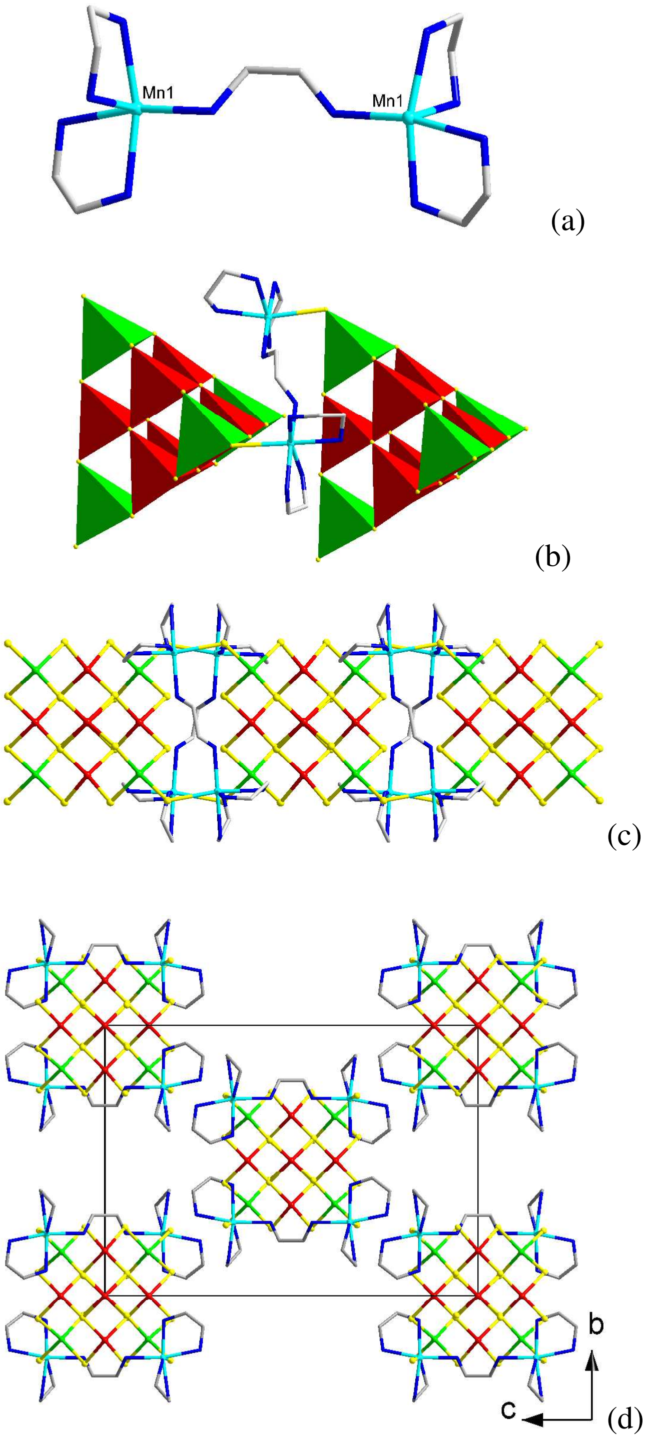

Fig. 2. A close-up view of the $[Mn_{2}(en)_{5}]^{4+}$ complex (a), connection mode between $[Mn_{2}(en)_{5}]^{4+}$ complex and $[Mn_{2}Ga_{4}Sn_{4}S_{20}]^{8-}$ T3 nanocluster (b), the 1D $[Mn_{2}(en)_{5}]MnGa_{2}Sn_{2}S_{10}$ chain along the c-axis (c), and the packing manner of the 1D chains viewed along the a-axis (d) in compound **1**.

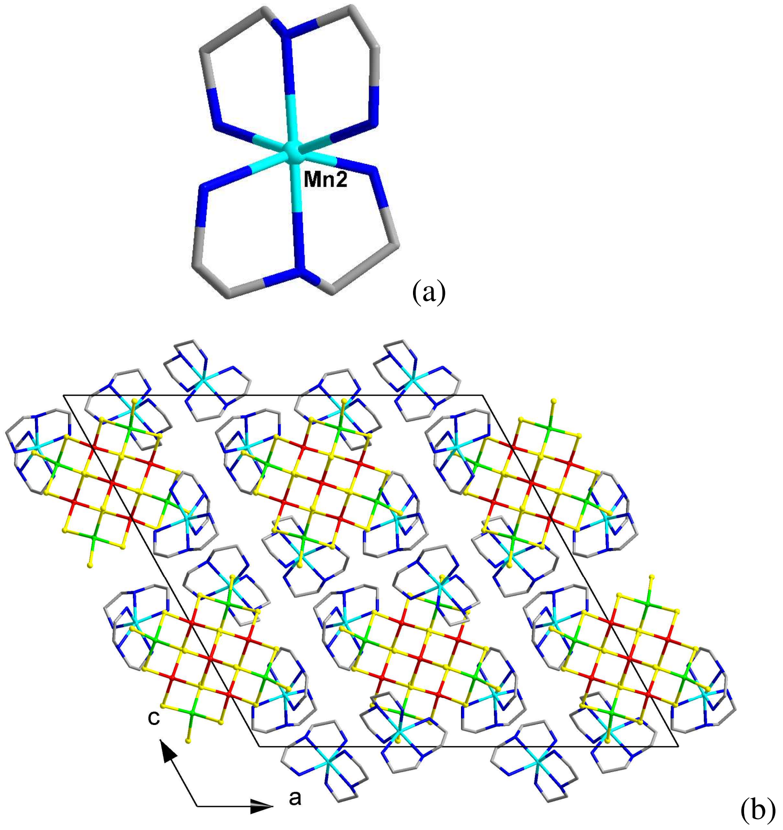

Fig. 3. View of the $[Mn(dien)_2]^{2+}$ complex (a), and the crystal structure of compound **2** along the b-axis (b).

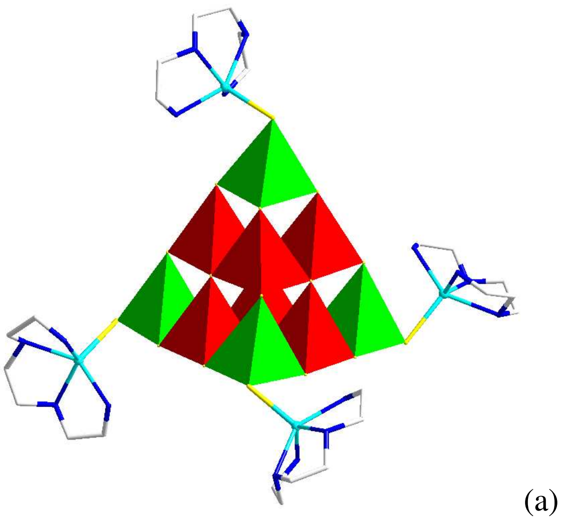
(a)

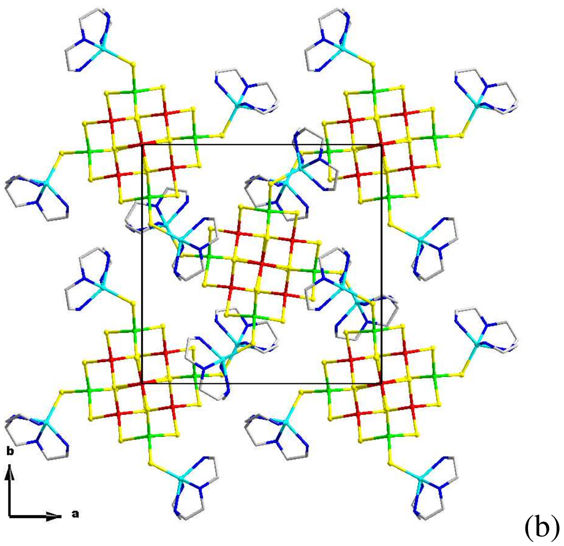

(b)

Fig. 4. View of the connecting mode between the $[Mn(teta)]^{2+}$ complex and $[Mn_2Ga_4Sn_4S_{20}]^{8-}$ T3 nanocluster (a), and the crystal packing of **3** viewed down the c-axis (b).

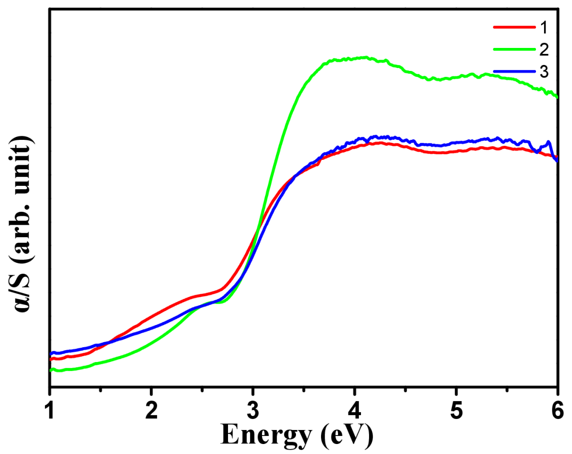

Fig. 5. Solid-state optical absorption spectra of compounds **1-3**

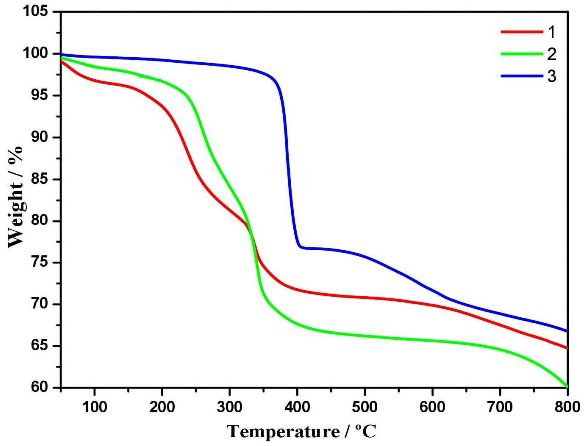

Fig. 6. Thermogravimetric curves for compounds **1-3**

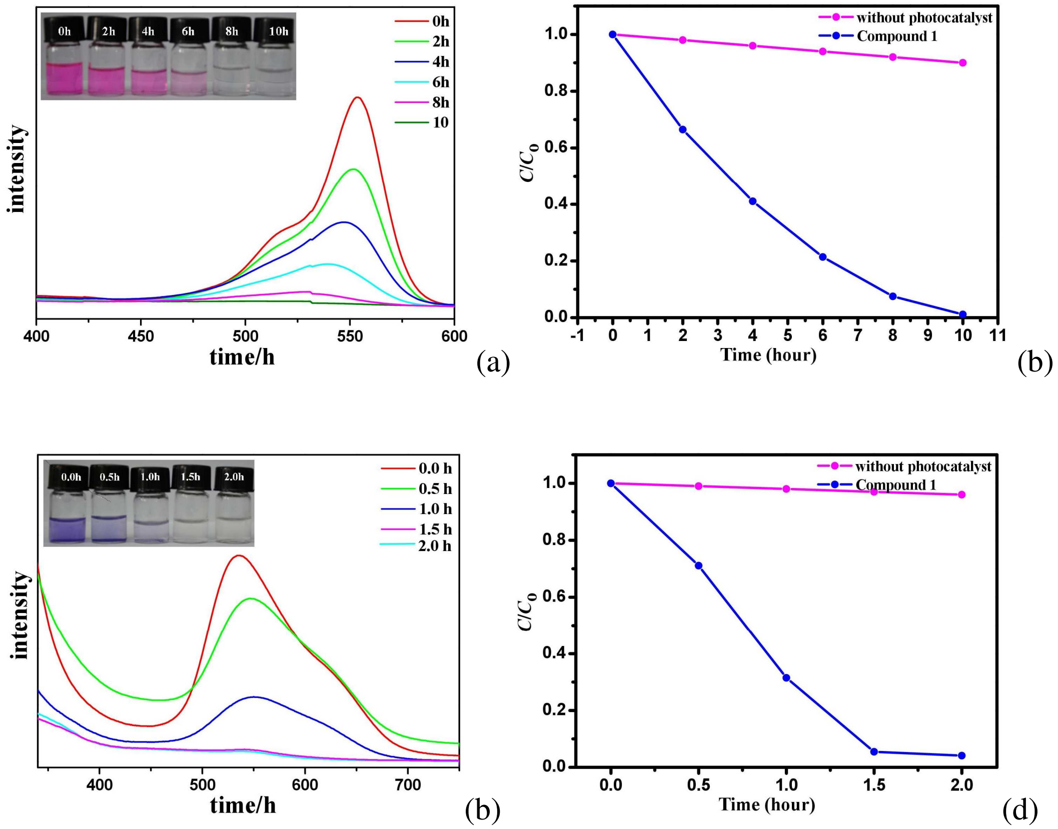

Fig. 7. Absorption spectra of solution of RhB (a-b) and CV (c-d) in the presence of compound **1** under exposure to visible light.